Journal of Radiation Research and Applied Sciences 18 (2025) 101452

Contents lists available at ScienceDirect

Journal of Radiation Research and Applied Sciences

journal homepage: www.journals.elsevier.com/journal-of-radiation-research-and-applied-sciences

Bioconvective flow of Casson-Micropolar nanofluid over bidirectional surface with radiation thermophoretic and Cattaneo-Christov model

Rejab Hajlaoui [a], Aaqib Majeed [b], Sami Ullah Khan [c], Mohamed Mahdi Boudabous [a], Alaa Chabir [d], Ali Chamkha [e], Lioua Kolsi [f,*]

[a] Department of Information and Computer Science, College of Computer Science and Engineering, University of Hai'l, Hai'l City, Saudi Arabia
[b] Department of Mathematics, The University of Faisalabad, Sargodha Road, University Town Faisalabad, 38000, Pakistan
[c] Department of Mathematics, Namal University, Mianwali, 42250, Pakistan
[d] Department of Computer Engineering, College of Computer Science and Engineering, University of Ha'il, Ha'il City, Saudi Arabia
[e] Faculty of Engineering, Kuwait College of Science and Technology, Doha District, 35004, Kuwait
[f] Department of Mechanical Engineering, College of Engineering, University of Ha'il, Ha'il City, 81451, Saudi Arabia

ARTICLE INFO

Keywords:
Nanofluid
Casson-micropolar nanofluid
Cattaneo-christov model
Thermal radiation
Chemical reaction

ABSTRACT

Recent developments in nanotechnology identifies the novel role of nanomaterials in upgrading the transport phenomenon of heat and mass transfer analysis. The significance of nanofluid is widely examined in energy enhancement, solar and nuclear systems, cooling applications, extrusion processes and various biomedical applications. This investigation contributes to bioconvective flow of Casson-Micropolar nanofluid due to porous bidirectional stretched surface. Unlike traditional models, a non-Fourier approach (Cattaneo-Christov model) is implemented to analyze the transport problem. The radiated effects and chemical reaction consequences are adopted to modify the model. The numerical computations are performed with help of shooting technique. It has been observed that the micro-rotational velocity due to porosity parameter while stretching parameter shows opposite results. The heat transfer impact enhances due to porosity parameter and micropolar fluid constant. The demonstrated results due to variation of flow parameters preserves applications in optimizing heat transfer efficiency, cooling impact, biofuels, fertilizers etc.

1. Introduction

The nanomaterials express the modified class of conventional fluids, exhibiting more superior thermal impact and stable conducting features. The source of nanofluids are based on dispersion of nanoscale particles to base liquids. Subject to tiny size and higher surface area, the decomposition of metallic particles to base materials enhances the thermal conductivity and other conducting performances. The nanomaterials show size-dependent refection, which confirms their magnetic, unique optical and thermal features. The utilization of nanofluids offer efficient energy transport, enhanced heat dissipation and impressive thermal management. The significance of nanofluid are examined in increasing lubrication, reducing wear and tear in mechanical processes and controlled viscosity, confirming applications in different industrial systems. The research on nanofluid has grown rapid interest and present novel applications in enhancing efficiency of HVAC systems, controlling the cooling processes in microchips and electronic systems. The applications of nanofluids in renewable energy presents applications in solar collectors. In modern nuclear medical, the nanoparticles present applications in the diagnostic imagining, hyperthermia treatment and drug delivery. The pioneer work on nanofluid was performed by Choi (Choi & Eastman, 1995). Hayat et al. (Hayat et al., 2020) determined the unsteady trnaport of nanofluid under the assumptions of variable thermal features. Thriveni and Mahanthesh (Thriveni & Mahanthesh, 2021) investigated the fluctuation of heat transfer subject to annulus flow of nanofluid. Rajput et al. (Rajput et al., 2022) visualized the unsteady flow of nanofluid to analyze the heat transfer effects. Abdal et al. (Abdal et al., 2021) focused to thermal aspects of nanofluid due to elongation of cylinder with porous medium. The preduction of thermal phenomenon in revolving canal filled with nanoparticles was explained by Mahanthesh et al. (Mahanthesh et al., 2016). Mahian et al. (Mahian et al., 2021) analyzed the thermal applications of nanoparticles to enhance

* Corresponding author.
E-mail addresses: raj.mohamed@uoh.edu.sa (R. Hajlaoui), mjaaqib@gmail.com (A. Majeed), sk_iiu@yahoo.com (S.U. Khan), moh.mahd@uoh.edu.sa (M.M. Boudabous), alaa.chabir@uoh.edu.sa (A. Chabir), a.chamkha@kcst.edu.kw (A. Chamkha), l.kolsi@uoh.edu.sa (L. Kolsi).

https://doi.org/10.1016/j.jrras.2025.101452
Received 24 January 2025; Received in revised form 16 March 2025; Accepted 19 March 2025
Available online 26 March 2025

heat transfer performances of renewable systems. Zaheer et al. (Zaheer et al., 2024) responded the stagnation point analysis for buoyancy driven flow of nanofluid. The analytical simulations are problem were performed with homotopy analysis scheme. Chabani et al. (Chabani et al., 2022) performed the heat transfer in trapezoidal enclosure for convective flow. The role of heat absorption in hybrid nanofluid has been evaluated by Mashhadian et al. (Mashhadian et al., 2021) Ali et al. (Ali et al., 2021) examined the rotatory flow of nanofluid numerically via finite element technique. Baazeem et al. (Baazeem et al., 2023) developed mathematical model for unsteady transport of nanofluid with additional Darcy-Forchheimer impact. Ramasekhar et al. (Ramasekhar et al., 2023) used the semi-analytical scheme to analyze the heat transfer performances in rotatory flow of nanofluid. Solar collectors applications with interaction of aluminum nanoparticles was revealed by Chukami et al. (Chukami et al., 2023). Batool et al. (Batool et al., 2023) expresses the viscous dissipation flow of nanofluid due to extension of surface. Mahmood et al. (Mahmood et al., 2022) focused to thermal aggregation of nanoparticles with viscous dissipation consequences. Nasir et al. (Nasir et al., 2023) contributed to investigation of heat transfer due to mixed convective flow of nanoparticles. Das et al. (Das et al., 2025) intended the heat transfer in vibrated channel containing the hybrid nanoparticles under rapid temperature constraints. Karmakar et al. (Karmakar et al., 2025) focused the Riga surface flow of nanofluid due to vibrated Riga surface. The thermal analysis subject to radiative flow of platinum-cerium oxide-water nanofluid was examined by Das et al. (Das et al., 2024). Karmakar et al. (Karmakar et al., 2024) visualized the weakly ionized flow of nanofluid in Riga channel with electromagnetic rotation. Loganathan et al. (Loganathan, Choudhary, et al., 2025) predicted the entropy generation in Riga supported flow of nanofluid with implementation of non-Fourier approach. The investigation for heat transfer with utilization of Williamson nanofluid was observed by Loganathan et al. (Loganathan, Thamaraikannan, et al., 2025). Senthilvadivu et al. (Senthilvadivu et al., 2024) analyzed the thermal energy transport due to suspension of ethylene glycol base nanofluid. Eswaramoorthi et al. (Eswaramoorthi et al., 2025) focused the thermal prediction of carbon nanofluid with ohmic heating effects. Sarfraz and Khan (Sarfraz et al., 2023a) reported the Homann flow of nanofluid due to biaxially moving surface. Yasir et al. (Yasir et al., 2023) developed mathematical model for non-inertial flow of Oldroyd-B nanofluid. Ahammad et al. (Ameer et al., 2022) addressed the convective transport of nanofluid for stagnation point assessment. Comparative heat transfer due to Xue and Hamilton–Crosser nanofluid models was investigated by Sarfraz et al. (Sarfraz, Yasir, & Khan, 2023). Muhammad et al. (Muhammad et al., 2025) intended examined thermal efficiency of hybrid nanofluid by performing statistical analysis.

In various classes of non-Newtonian materials, the micropolar fluid is famous category which contributes the understanding of novel microstructure features. In contrasting to traditional nonlinear models, the micropolar fluid exhibits the rotational behavior and microstructural impact of fluid particles. The rheology of micropolar fluid is important for analyzing the angular velocity and micro-rotational suspension of particles for understanding internal dynamic of complex materials. The significant applications of micropolar fluid has been analyzed in diverse range of fields. In liquid crystals, the micropolar fluid help in understanding of rotational characteristics of elongated molecules and anisotropic materials. In colloidal decompositions, the micropolar fluids accounts the rotational movement of suspended colloids. The human blood properties can also be justified with help of micropolar fluid. In biomedical engineering, the micropolar dynamics can be followed to model in tissues engineering, diagnostics devices and drug delivery processes where the micro-scale materials crucial for augmenting the performances. Guedri et al. (Guedri et al., 2023) presented the aggregation of micropolar nanofluid subject to shrining surface flow under the influence of thermal radiation. Rana et al. (Rana et al., 2020) explained the improved heat transfer aspects subject to micropolar nanofluid. Vertically supported flow of micropolar nanofluid with heat transfer impact was predicted by Khan et al. (Khan et al., 2021). Habib et al. (Habib et al., 2021) analyzed the utilization of microbes in nanofluid flow confined by stretching surface. Abbas et al. (Abbas et al., 2024) investigated the micropolar nanofluid driven by Riga electromagnetic surface. Pandey et al. (Pandey & Chandra, 2020) focused to study of rotational effects governed by micropolar fluid due to propagation of waves. Ali et al. (Ali et al., 2020) used the magnetic dipole effects while performing the heat and mass transfer due to micropolar fluid. Karvelas et al. (Karvelas et al., 2020) predicted the insight to micropolar flow by claiming the fibrous hydraulic permeability applications. Majeed et al. (Majeed et al., 2024) discussed the bidirectional stretching Riga surface flow of Casson-micropolar and nanofluid. However, this analysis was performed by utilizing the traditional Fourier approach.

Despite extensive investigations on bioconvective flow of nanofluid due bidirectional stretching surface, it has been analyzed that assessment of heat and mass transfer due to bioconvective flow of radiated Casson-Micropolar nanofluid has not be explored yet. This research aims to presents the heat and mass transfer aspects in magnetized Casson-Micropolar nanofluid with suspension of microorganisms. A source of flow is bidirectional stretched surface subject to porous media. The bidirectional stretched surface flow of nanomaterials is novel with realistic industrial, engineering and biomedical applications like extrusion processes, manufacturing systems, polymers, coating phenomenon and bio-fluid transport. The Cattaneo-Christov model is incorporated to model the problem. The assessment of heat transfer is performed by incorporating the radiated effects. The concentration equation is updated by utilizing the chemical reaction consequences. A complex system of equations has been developed which is solved via shooting algorithm. The physical impact of problem is presented graphically due to variation of modeled parameters.

2. Flow assumptions and governing equations

A bidirectional stretched surface flow of Casson-Micropolar nanofluid containing the microorganisms have been studded. Cartesian plane is used to model the problem. The flow configuration is presented in Fig. 1. The governing equations are obtained in view of following flow assumptions.

- ❖ A steady and laminar flow of Casson-Micropolar nanofluid with suspension of microorganisms has been considered due to bidirectional porous stretching surface.
- ❖ The velocity components u, v and w are considered along x, y and z, directions, respectively.
- ❖ The bidirectional velocities of stretching surface are expressed with $u = U_w = U_0 \exp\left[\frac{x+y}{L}\right], v = V_w = V_0 \exp\left[\frac{x+y}{L}\right]$.

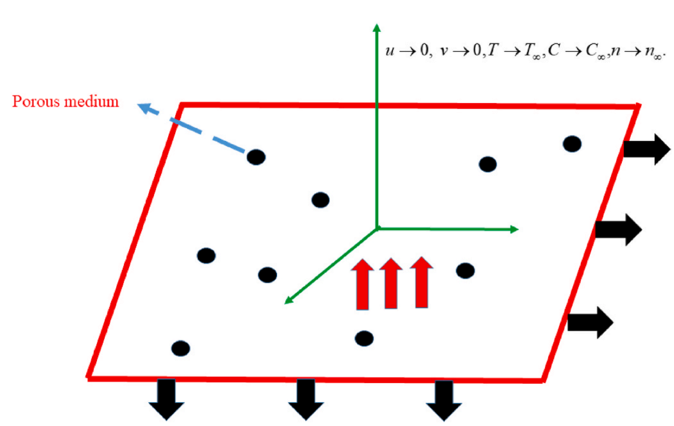

Fig. 1. Flow configuration of the problem.

- Normal magnetic force effects are considered. The induced magnetic force features are ignored under small magnetic Reynolds number assumptions.
- The extension in heat and mass transfer equations is suggested with help of Cattaneo-Christov approach.
- The energy equation retaining the thermal radiation consequences while chemical reaction features are adopted in heat and concentration equation, respectively.
- Let N be micro-rotation, T defines the temperature, C explaining the dilute concentration and n be microorganisms density. Moreover, N_1 and N_2 represents the micro-angular speed, T_∞ is the free stream temperature, C_∞ represents the ambient stream concentration while n_∞ is ambient microorganism density.

Following all these assumptions, the problem is expressed with help of following set of equations (Majeed et al., 2024):

$$\frac{\partial u}{\partial x}+\frac{\partial v}{\partial y}+\frac{\partial w}{\partial z}=0, \tag{1}$$

$$u\frac{\partial u}{\partial x}+v\frac{\partial u}{\partial y}+w\frac{\partial u}{\partial z}=\left(1+k+\frac{1}{\omega}\right)\frac{\partial^2 u}{\partial z^2}-\frac{K}{\rho_f}\left(\frac{\partial N_2}{\partial z}\right)-\frac{\sigma B_0^2 u}{\rho_f}-\frac{\upsilon_f u}{K^*}, \tag{2}$$

$$u\frac{\partial v}{\partial x}+v\frac{\partial v}{\partial y}+w\frac{\partial v}{\partial z}=\left(1+k+\frac{1}{\omega}\right)\frac{\partial^2 v}{\partial z^2}-\frac{K}{\rho_f}\left(\frac{\partial N_1}{\partial z}\right)-\frac{\sigma B_0^2 v}{\rho_f}-\frac{\upsilon_f v}{K^*}, \tag{3}$$

$$\begin{aligned}u\frac{\partial T}{\partial x}+v\frac{\partial T}{\partial y}+w\frac{\partial T}{\partial z}=&\frac{K_f}{(\rho c)_f}\frac{\partial^2 T}{\partial z^2}-\lambda_0\Bigg[u^2\frac{\partial^2 T}{\partial x^2}+v^2\frac{\partial^2 T}{\partial y^2}+w^2\frac{\partial^2 T}{\partial z^2}+2uv\frac{\partial^2 T}{\partial x\partial y}\\&+2vw\frac{\partial^2 T}{\partial y\partial z}+2uw\frac{\partial^2 T}{\partial x\partial z}+\left(u\frac{\partial u}{\partial x}+v\frac{\partial u}{\partial y}+w\frac{\partial u}{\partial z}\right)\frac{\partial T}{\partial x}\\&+\left(u\frac{\partial v}{\partial x}+v\frac{\partial v}{\partial y}+w\frac{\partial v}{\partial z}\right)\frac{\partial T}{\partial y}+\left(u\frac{\partial w}{\partial x}+v\frac{\partial w}{\partial y}+w\frac{\partial w}{\partial z}\right)\frac{\partial T}{\partial z}\Bigg]\\&+\frac{(\rho c)_p}{(\rho c)_f}\left[D_B\frac{\partial^2 C}{\partial z^2}\frac{\partial T}{\partial z}+\frac{D_T}{T_\infty}\left(\frac{\partial T}{\partial z}\right)^2\right]-\frac{1}{(\rho c)_f}\left(\frac{\partial q_r}{\partial z}\right)\end{aligned} \tag{4}$$

$$\begin{aligned}u\frac{\partial C}{\partial x}+v\frac{\partial C}{\partial y}+w\frac{\partial C}{\partial z}=&D_B\frac{\partial^2 C}{\partial z^2}+\frac{D_T}{T_\infty}\frac{\partial^2 T}{\partial z^2}-\lambda_1\Bigg[u^2\frac{\partial^2 C}{\partial x^2}+v^2\frac{\partial^2 C}{\partial y^2}+w^2\frac{\partial^2 C}{\partial z^2}\\&+2uv\frac{\partial^2 C}{\partial x\partial y}+2vw\frac{\partial^2 C}{\partial y\partial z}+2uw\frac{\partial^2 C}{\partial x\partial z}+\left(u\frac{\partial u}{\partial x}+v\frac{\partial u}{\partial y}+w\frac{\partial u}{\partial z}\right)\frac{\partial C}{\partial x}\\&+\left(u\frac{\partial v}{\partial x}+v\frac{\partial v}{\partial y}+w\frac{\partial v}{\partial z}\right)\frac{\partial C}{\partial y}+\left(u\frac{\partial w}{\partial x}+v\frac{\partial w}{\partial y}+w\frac{\partial w}{\partial z}\right)\frac{\partial C}{\partial z}\Bigg]-K_*(C-C_\infty)\end{aligned} \tag{5}$$

$$u\frac{\partial n}{\partial x}+v\frac{\partial n}{\partial y}+w\frac{\partial n}{\partial z}=D_m\left(\frac{\partial^2 n}{\partial z^2}\right)-\frac{\overline{b}w_c}{(C-C_\infty)}\frac{\partial}{\partial z}\left(n\frac{\partial C}{\partial z}\right), \tag{6}$$

$$u\frac{\partial N_1}{\partial x}+v\frac{\partial N_1}{\partial y}+w\frac{\partial N_1}{\partial z}=\frac{\gamma}{\rho_f j}\frac{\partial^2 N_1}{\partial z^2}-\frac{2KN_1}{\rho_f j}-\frac{K}{\rho_f j}\frac{\partial v}{\partial z}, \tag{7}$$

$$u\frac{\partial N_2}{\partial x}+v\frac{\partial N_2}{\partial y}+w\frac{\partial N_2}{\partial z}=\frac{\gamma}{\rho_f j}\frac{\partial^2 N_2}{\partial z^2}-\frac{2KN_2}{\rho_f j}-\frac{K}{\rho_f j}\frac{\partial u}{\partial z}, \tag{8}$$

with σ (electric conductivity), ρ_f (density), K (micropolar fluid coefficient), ω (Casson fluid coefficient), q_r (radiated coefficient), K^* (porous media coefficient), λ_0 (thermal relaxation coefficient), D_T (thermophoretic coefficient), K_* (reaction coefficient), j (microintertia density), D_m (microorganisms diffusivity), $\overline{b}$ (chemotaxis constant) and w_c (maximum cells speed).

The boundary conditions are (Majeed et al., 2024):

$$\left.\begin{aligned}&u=U_w=U_0\exp\left[\frac{x+y}{L}\right],v=V_w=V_0\exp\left[\frac{x+y}{L}\right],w=0,\\&T=T_w=T_\infty+T_o\exp\left[\frac{A(x+y)}{2L}\right],C=C_w=C_\infty+C_o\exp\left[\frac{B(x+y)}{2L}\right],\\&n=n_w=n_\infty+n_0\exp\left[\frac{D(x+y)}{2L}\right],\\&N_1=\frac{1}{2}\frac{\partial v}{\partial z},N_2=-\frac{1}{2}\frac{\partial u}{\partial z}\ \text{as}\quad z=0.\end{aligned}\right\} \tag{9}$$

$$u\to 0,v\to 0,T\to T_\infty,C\to C_\infty,n\to n_\infty,N_1\to 0,N_2\to 0\ as\ Z\to\infty. \tag{10}$$

Above defined boundary conditions are associated to the stretched surface flows. Physically, these constraints express the velocity, temperature, concentration and microorganisms behavior within the surface and fluid. Such constraints are important in industrial processes like metal forming, polymer extrusion, coating flows etc.

2.1. Dimensionless variables

The new endorsed variables are (Majeed et al., 2024):

$$u=U_W=U_0\ \exp\left[\frac{x+y}{L}\right]f'(\eta), \tag{11}$$

$$v=V_W=V_0\ \exp\left[\frac{x+y}{2L}\right]g'(\eta), \tag{12}$$

$$w=-\sqrt{\frac{\upsilon_f U_0}{2L}}\exp\left[\frac{x+y}{L}\right][f(\eta)+\eta f'(\eta)+g(\eta)+\eta g'(\eta)], \tag{13}$$

$$T=T_W=T_\infty+T_o\ \exp\left[\frac{A(x+y)}{2L}\right]\theta(\eta), \tag{14}$$

$$C=C_W=C_\infty+C_o\ \exp\left[\frac{B(x+y)}{2L}\right]\varphi(\eta), \tag{15}$$

$$n=n_W=n_\infty+n_0\ \exp\left[\frac{D(x+y)}{2L}\right]\chi(\eta), \tag{16}$$

$$N_1=\sqrt{\frac{U_0^3}{2\upsilon_f L}}\exp\left[\frac{3(x+y)}{2L}\right]R(\eta), \tag{17}$$

$$N_2=\sqrt{\frac{U_0^3}{2\upsilon_f L}}\exp\left[\frac{3(x+y)}{2L}\right]Q(\eta) \tag{18}$$

$$\eta=\sqrt{\frac{U_0}{2\upsilon_f L}}\exp\left[\frac{x+y}{2L}\right]z \tag{19}$$

where A,B and D are the temperature, concentration, and motile exponents respectively. Moreover, $T_0,C_0,$ and n_0 are the constants. The new dimensionless system is:

$$\left(1+\alpha+\frac{1}{\omega}\right)f'''-\alpha Q'+(f+g)f''-(f'+g')f'-\left(M+\gamma_p\right)f'=0, \tag{20}$$

$$\left(1+\alpha+\frac{1}{\omega}\right)g'''-\alpha R'+(f+g)g''-(f'+g')g'-\left(M+\gamma_p\right)g'=0, \tag{21}$$

$$\begin{aligned}&\left(1+\frac{4}{3}R+Pr\,\lambda_T(f+g)^2\right)\theta''+\Pr\left[A(f+g)\theta'-(f'+g')\theta+Nb\theta'\phi'+Nt(\theta')^2\right]\\&+Pr\,\lambda_T\Big[(\eta f'+\eta g'+f+g+2Af+2Ag)(f'+g')\theta'\\&-A\left\{(A+2)\left(f'^2+g'^2+2f'g'\right)-(ff''+fg''+f''g+gg'')\right\}\theta\Big]=0,\end{aligned} \tag{22}$$

$$\phi'' + Sc[(f+g)\phi' - B(f'+g')\phi - kr\phi] - Sc\lambda_C\Big[(\eta f' + \eta g' + f + g + 2Af + 2Ag)(f'+g')\phi' - A\Big\{(A+2)\Big(f'^2 + g'^2 + 2f'g'\Big) - (ff'' + fg'' + f''g + gg'')\Big\}\phi\Big] + \frac{Nt}{Nb}\theta'' = 0, \tag{23}$$

$$\chi'' + Sb[(f+g)\chi' - D(f'+g')\chi] - Pe[(\sigma+\chi)\phi'' + \chi'\phi'] = 0, \tag{24}$$

$$\Big(1+\frac{\alpha}{2}\Big)R'' + (f+g)R' - 3(f'+g')R - 2\alpha R - \alpha g'' = 0, \tag{25}$$

$$\Big(1+\frac{\alpha}{2}\Big)Q'' + (f+g)Q' - 3(f'+g')Q - 2\alpha Q - \alpha f'' = 0, \tag{26}$$

with boundary conditions (Majeed et al., 2024):

$$f(0)=0, g(0)=0, f'(0)=1, g'(0)=\lambda, \theta'(0) = -\beta_h(1-\theta(0)), \phi'(0) = -\beta_C(1-\phi(0)), \chi'^{(0)} = -\beta_X(1-\chi(0)), R(0) = ng''(0), Q(0) = -nf''(0), \tag{27}$$

$$f'(\infty)\to 0, g'(\infty)\to 0, \theta(\infty)\to 0, \phi(\infty)\to 0, \chi(\infty)\to 0, R(\infty)\to 0, Q(\infty)\to 0. \tag{28}$$

with micropolar parameter (α), Hartmann number (M), stretching parameter (λ), Prandtl number (Pr), Brownian motion (Nb), thermophoresis parameter (Nt), Schmidt number (Sc), and Peclet number (Pe)

$$\alpha=\frac{k}{\mu_f}, M=\frac{2\sigma B_0^2 L}{\rho_f U_w}, \lambda=\frac{V_0}{U_0}, Pr=\frac{\upsilon_f}{\alpha_f}, N_b=\frac{\tau D_B(C_W-C_\infty)}{\upsilon_f}, N_t=\frac{\tau D_T(T_W-T_\infty)}{\upsilon_f T_\infty},$$
$$S_c=\frac{\upsilon_f}{D_B}, Rr=\frac{K_s^2}{c}, N_f=\frac{T_f-T_\infty}{T_\infty}, E=\frac{E_a}{k_1 T_\infty}, Pe=\frac{\widetilde{b}D_m W_c}{D_B}, \lambda_T=\frac{\lambda_0 u_0 \exp((x+y)/L)}{2L}$$

2.2. Physical quantities

The wall shear force, Nusselt number, Sherwood number and motile density number are (Majeed et al., 2024):

$$Nu_x=\frac{xq_w}{k_f(T_w-T_\infty)}, Sh_x=\frac{xq_m}{k_f(C_w-C_\infty)}, Q_{nx}=\frac{xq_n}{D_m n_w} \tag{29}$$

where $q_w = -K_f\left(\frac{\partial T}{\partial z}\right)_{z=0}$, $q_m = -D_B\left(\frac{\partial C}{\partial z}\right)_{z=0}$ and $q_n = -D_m\left(\frac{\partial n}{\partial z}\right)_{z=0}$ are the wall heat flux, wall mass flux and microorganism flux from the stretching surface respectively. The dimensionless form is:

$$\left(\frac{Re_x}{2}\right)^{-\frac{1}{2}}\frac{L}{x}Nu_x = -\left(1+\frac{4}{3}Nr\right)\theta'(0), \tag{30}$$

$$\left(\frac{Re_x}{2}\right)^{-\frac{1}{2}}\frac{L}{x}Sh_x = -\phi'(0), \tag{31}$$

$$\left(\frac{Re_x}{2}\right)^{-\frac{1}{2}}\frac{L}{x}Q_{nx} = -\chi'(0). \tag{32}$$

3. Numerical simulations

Coupled system of equation is numerically solved with shooting technique. Shooting method is based on transferring the higher order system to first order problem. Following new variables are introduced to attains the first order relations:

$$\left.\begin{array}{c} f=z_1, f'=z_2, f''=z_3, f'''=z_3', g=z_4, g'=z_5, g''=z_6, g'''=z_6', \\ \theta=z_7, \theta'=z_8, \theta''=z_8', \phi=z_9, \phi'=z_{10}, \phi''=z_{10}', \chi=z_{11}, \chi'=z_{12}, \chi''=z_{12}', \\ R=z_{13}, R'=z_{14}, R''=z_{14}', Q=z_{15}, Q'=z_{16}, Q''=z_{16}' \end{array}\right\} \tag{33}$$

Replacing above quantities in dimensionless equations:

$$z_3'=\frac{1}{\left(1+\alpha+\frac{1}{\omega}\right)}\Big[\alpha z_{16} - (z_1+z_4)z_3 + (z_2+z_5)z_2 + \Big(M+\gamma_p\Big)z_2\Big], \tag{34}$$

$$z_6'=\frac{1}{\left(1+\alpha+\frac{1}{\omega}\right)}\Big[\alpha z_{14} - (z_1+z_4)z_6 + (z_2+z_5)z_5 + \Big(M+\gamma_p\Big)z_5\Big], \tag{35}$$

$$z_8'=\frac{1}{\left(1+\frac{4}{3}R+Pr\,\lambda_T(f+g)^2\right)}\Big[-\Pr\Big[A(z_1+z_4)z_8 - (z_2+z_5)z_7 + Nbz_8z_{10} + Nt(z_8)^2\Big] - Pr\,\lambda_T\Big[(\eta z_2+\eta z_5+z_1+z_4+2Az_1+2Az_4)(z_2+z_5) z_8 - A\Big\{(A+2)\Big((z_2)^2+(z_5)^2+2z_2z_5\Big) - (z_1z_3+z_1z_6+z_3z_4+z_4z_6)\Big\}z_7=0\Big], \tag{36}$$

$$z_{10}' = -Sc[(z_1+z_4)z_{10} - B(z_2+z_5)z_9 - krz_9] + Sc\lambda_C\Big[(\eta z_2+\eta z_5+z_1+z_4 + 2Az_1+2Az_4)(z_2+z_5)z_{10} - A\Big\{(A+2)\Big((z_2)^2+(z_5)^2+2z_2z_5\Big) - (z_1z_3+z_1z_6+z_3z_4+z_4z_6)\Big\}z_9\Big] - \frac{Nt}{Nb}z_8', \tag{37}$$

$$z_{12}' = -Sb[(z_1+z_4)z_{12} - D(z_2+z_5)\chi] + Pe\big[(\sigma+z_{11})z_{10}' + z_{10}z_{12}\big], \tag{38}$$

$$z_{14}'=\frac{1}{\left(1+\frac{\alpha}{2}\right)}[-(z_1+z_4)z_{14} + 3(z_2+z_5)z_{13} + 2\alpha z_{13} + \alpha z_6], \tag{39}$$

$$z_{16}'=\frac{1}{\left(1+\frac{\alpha}{2}\right)}[-(z_1+z_4)z_{16} + 3(z_2+z_5)z_{15} + 2\alpha z_{15} + \alpha z_3], \tag{40}$$

with:

$$z_1(0)=0, z_4(0)=0, z_2(0)=1, z_5(0)=\lambda, z_8(0) = -\beta_h(1-z_7(0)), z_{10}(0) = -\beta_C(1-z_9(0)), z_{12}(0) = -\beta_X(1-z_{11}(0)), z_{13}(0) = nz_6(0), z_{15}(0) = -nz_3(0), \tag{41}$$

$$z_2(\infty)\to 0, z_5(\infty)\to 0, z_7(\infty)\to 0, z_9(\infty)\to 0, z_{11}(\infty)\to 0, z_{13}(\infty) \to 0, z_{15}(\infty)\to 0. \tag{42}$$

4. Solution verification

The numerical results are now validated in Table 1 by comparing with benchmark investigation of Ariel (Ariel, 2007) under some limiting case. Both studies confirmed close agreement which guaranteed the solution accuracy.

Table 1
Comparison of simulated numerical data with Ariel (Ariel, 2007) when $\alpha = \gamma_p = 0$ and $\omega\to\infty$.

parameter	Ariel (Ariel, 2007)		Present numerical results	
λ	$-f''(0)$	$-g''(0)$	$-f''(0)$	$-g''(0)$
0.0	1.00000	0.00000	1.00000	0.00000
0.1	1.02025	0.06684	1.020244	0.066875
0.2	1.03949	0.14873	1.039513	0.148724

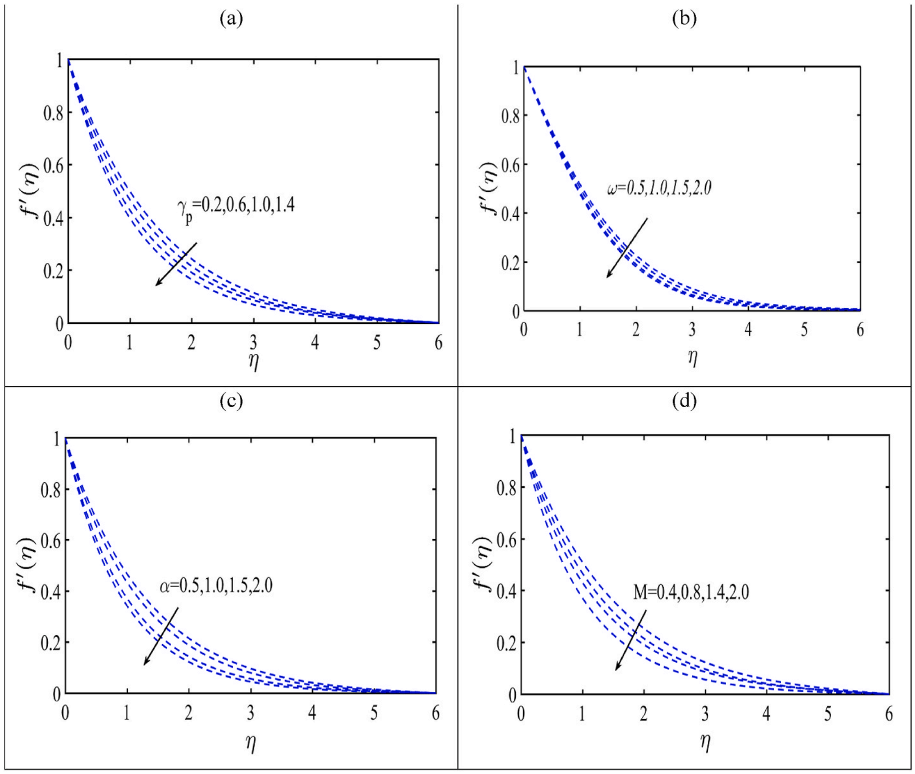

Fig. 2. (a–d): Variation of velocity profile $f'(\eta)$ due to impact of (a) porosity parameter (γ_p), (b) Casson fluid parameter (ω), (c) micropolar parameter (α), (d) Hartmann number (M).

5. Graphical results and discussion

In this section, the physical interpretation of results has been predicted and analyzed. The physical amplification of problem is assessed subject to variation of parameters. This section aims to explicate the fluctuation in velocity profiles ($f'(\eta), g'(\eta)$), micropolar functions ($Q(\eta)$, $R(\eta)$), temperature field $\theta(\eta)$, concentration profile $\phi(\eta)$ and motile microorganism profile $\chi(\eta)$ against the modeled parameters. Current

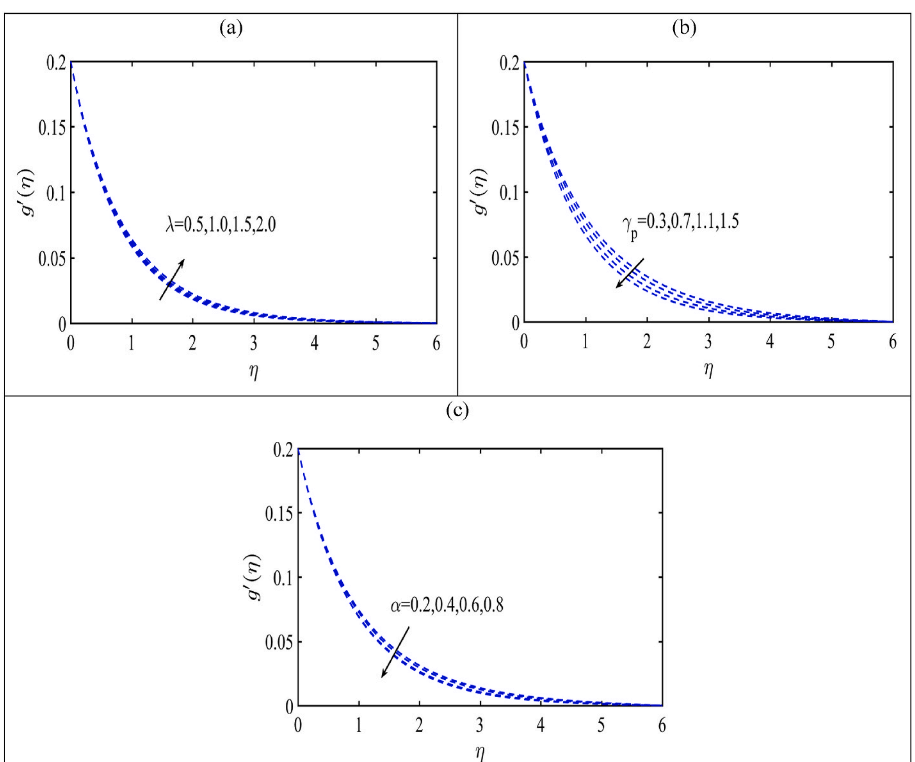

Fig. 3. (a–c): Variation of velocity profile $g'(\eta)$ due to impact of (a) stretching parameter (λ), (b) porosity parameter (γ_p) and (c) micropolar parameter (α).

flow problem is modeled under the theoretical flow assumptions, therefore, constant appropriate numerical values are assigned to involved flow parameters. Fig. 2(a) concentrates to understanding of velocity profile $f'(\eta)$ by entertaining the effects of porosity parameter γ_p. Upon enhancing numerical values of γ_p, a decrement in $f'(\eta)$ has been examined. The slower in velocity due to porosity constants indicate the presence of permeability of porous medium which controls the fluid velocity. Due to permeability of saturated porous space, the fluid velocity reduces. Fig. 2(b) perform the analysis for $f'(\eta)$ due to Casson fluid parameter (ω). The velocity profile reduces when ω increases. Physically, the Casson fluid model predicts the shear thinning consequences. In shear thinning effects, the viscosity of fluid declines when rate of shear force enhances which results in reduction of $f'(\eta)$. The results responded in Fig. 2(c) claim the influence of micropolar parameter (α) on $f'(\eta)$. The fluid profile gradually reduces when K gets larger numerical values. The micropolar fluid highlights the microstructural of fluid, describing the rotational movement of microelements within the fluid. Fig. 2(d) accounts the influence of Hartmann number (M) on $f'(\eta)$. Higher values of M leads to reduction of fluid velocity. Such observations are physically associated to Lorentz force which declines the velocity profile.

Fig. 3(a) reflects the influence of stretching parameter (λ) on $g'(\eta)$. Change in λ leads to enhancement of $g'(\eta)$. Fig. 3(b) describes the assessment of $g'(\eta)$ by enhancing porosity parameter (γ_p). Change in γ_p leads to reduction of $g'(\eta)$. This behavior is subject to increasing interaction between the fluid and porous medium. Higher impact of γ_p increases the drag of resistance between fluid particles resulting a decrement in velocity. In order to characterizes the observations for $g'(\eta)$ due to micropolar parameter (α), Fig. 3(c) is proposed. The change in α leads to decrement of $g'(\eta)$. The micropolar fluid parameter preserves the rotational impact of microelement within fluid, presenting prominent viscosity and resistance to the flow.

Fig. 4(a) evaluates the analysis for temperature profile $\theta(\eta)$ by increasing thermal relaxation parameter λ_T. The heat transfer declines when λ_T enhances. Since current mathematical model is based in implementation of Cattaneo-Christov model which account the finite thermal wave propagation, resulting delay in conduction phenomenon and controlling the temperature profile. Fig. 4(b) executes impact of porosity constant (γ_p) on the temperature profile $\theta(\eta)$. Upon γ_p enriches, boosted observations for $\theta(\eta)$ are revealed. The presence of porous

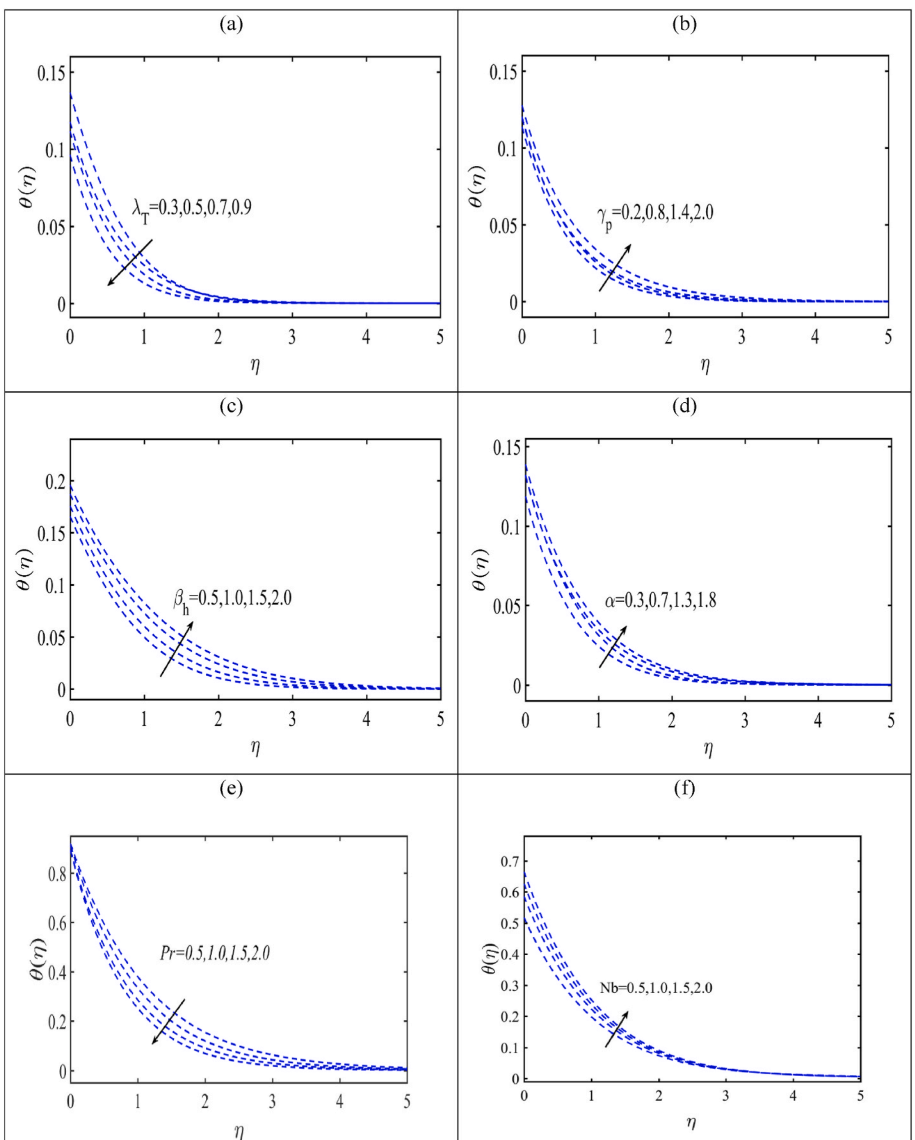

Fig. 4. (a–c): Temperature Profile $\theta(\eta)$ due to variation of (a) thermal relaxation parameter λ_T, (b) porosity constant (γ_p), (c) Biot number (β_h), (d) micropolar parameter (α), (e) Prandtl number (Pr) and (f) Brownian parameter (Nb).

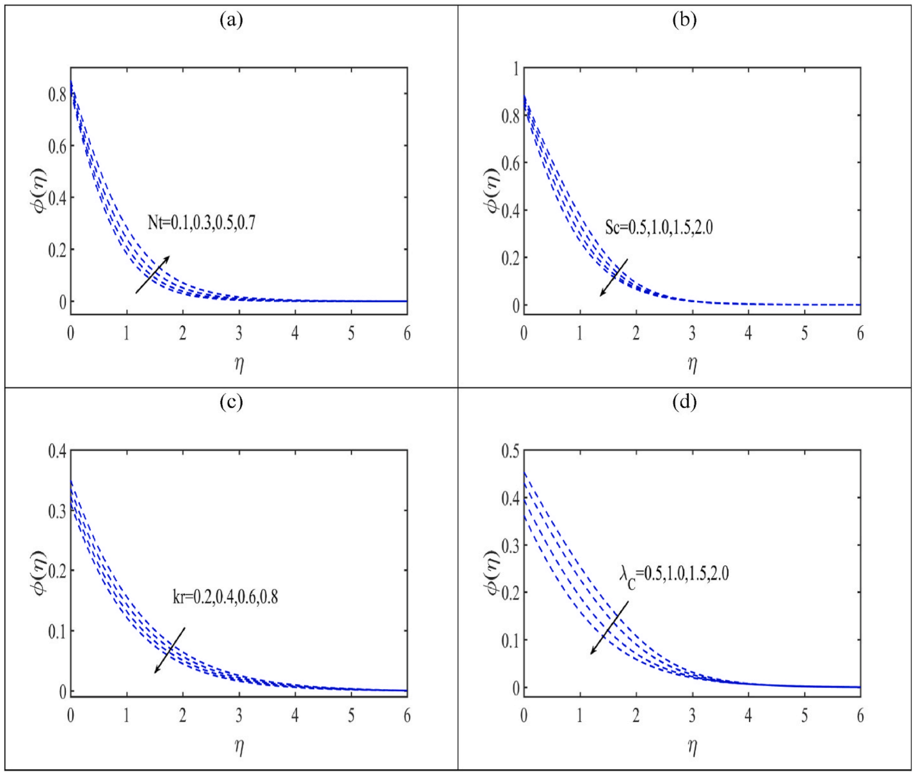

Fig. 5. (a–d): Profile of $\phi(\eta)$ due to (a) Nt (b) Sc (c) kr and (d) λ_C

media is effective to increases the heat transfer phenomenon. Such observations reveal importance in petroleum industry for recovery processes. In Fig. 4(c), the analysis is performed for temperature profile $\theta(\eta)$ due to larger variation of thermal Biot number (β_h). Increasing change in β_h enhances the heat transfer gradually. Physically, β_h attains a direct relationship with coefficient of heat transfer. The convective heat transfer enhances due to β_h. Fig. 4(d) concluding observations for $\theta(\eta)$ by varying micropolar parameter (α). Increment to α leads to enhancement of temperature profile. Fig. 4(e) demonstrates the outcome due to variation of Prandtl number (*Pr*) on $\theta(\eta)$. Subject to larger *Pr*, transfer of heat become slower sharply. Higher *Pr* correspond to smaller thermal diffusivity. The heat transfer condensed for lower thermal diffusivity. Such results are important for cooling processes in various electronics and engineering systems. In order to interpolates the significance of Brownian parameter (*Nb*) on $\theta(\eta)$, Fig. 4(f) is proposed. Larger *Nb* leads to rise in fluid temperature. Enhancement in *Nb* presents the random motion of nanofluid which contributes to improve the internal heat transfer within the fluid.

Fig. 5(a) discloses the variation in concentration profile $\phi(\eta)$ by increasing the thermophoresis parameter (*Nt*). An impressive rate of change is exhibited in $\phi(\eta)$ due to numerical variation of *Nt*. Physically, the thermophoresis phenomenon is subject to movement of fluid particles towards the cooler region. Such dispersion in thermophoresis phenomenon leads to enhancement of concentration profile. Fig. 5(b) evaluates the results for $\phi(\eta)$ corresponds to larger Schmidt number (*Sc*). A reduction in $\phi(\eta)$ is exhibited by enlarging *Sc*. Physically, increasing change in *Sc* leads to smaller mass diffusivity which turn down the concentration phenomenon. Fig. 5(c) justifies the features of chemical reaction parameter *kr* on $\phi(\eta)$. It is examined that $\phi(\eta)$ declines against higher values of *kr*. Fig. 5(d) analyzing the consequences of concentration relaxation number λ_C on $\phi(\eta)$. Upon larger variation of λ_C, the concentration field reduces.

Fig. 6(a and b) expresses the effects of micropolar fluid parameter α on angular velocity distribution $Q(\eta)$ and micro-rotation distribution $R(\eta)$. Enchantment in α leads to reduction of both profiles. These observations indicate that larger micropolar fluid parameter α offers

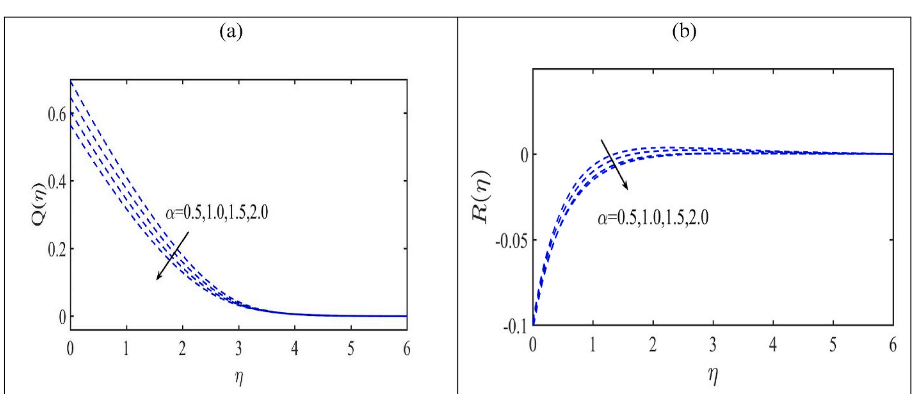

Fig. 6. (a–b): Effect of micropolar parameter (α) on (a) Q(η) and (a) R(η)

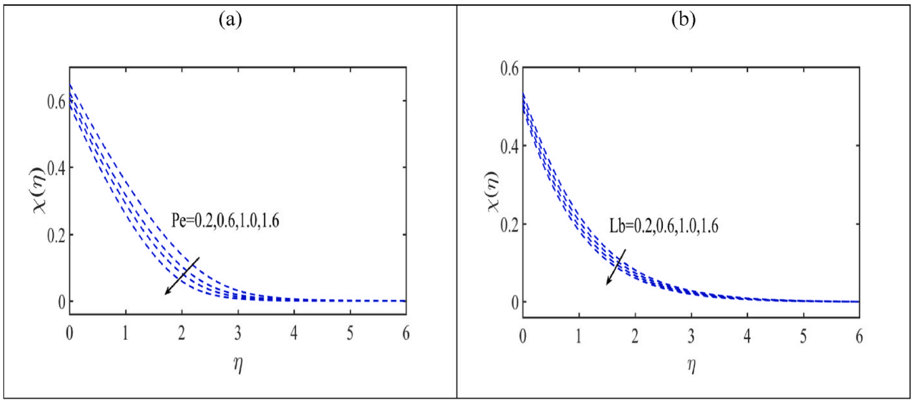

Fig. 7. (a–b): Profile of $\chi(\eta)$ due to (a) Pe (b).

Table 2
Variation of skin friction $(-f''(0))$, microrotation $(-g(0))$, temperature gradient $(-\theta'(0))$, concentration gradient $(-\phi'(0))$, and microorganism motility $(-\chi'(0))$ due to fluid parameters.

M	λ	Pr	γ_p	ω	α	$f''(0)$	$g(0)$	$-\theta'(0)$	$-\phi'(0)$	$-\chi'(0)$
0.2						1.97785	0.6561	1.26434	3.34533	3.16954
0.4						2.03365	0.6657	1.15767	3.26423	3.11433
0.6						2.05432	0.6752	1.04567	3.12342	3.07256
	0.2					1.97856	0.6561	1.15356	3.43533	3.16965
	0.4					2.05325	1.0084	1.29645	3.39654	3.23235
	0.8					2.13032	1.3761	1.29435	3.33085	3.29785
		0.4				1.12869	0.6561	1.10564	3.23533	3.16698
		0.8				1.27745	0.6561	1.13566	3.21345	3.15895
		1.2				1.54543	0.6561	1.17854	3.16977	3.14433
			0.2			1.97043	0.6561	1.11654	3.56311	3.16675
			0.6			2.03324	0.6657	1.10980	3.59043	3.16786
			1.0			2.08543	0.6752	1.09223	3.63353	3.17353
				0.2		1.97906	0.6561	1.11533	3.33666	3.16997
				1.2		1.83432	0.6230	1.09675	3.45430	3.17123
				1.8		1.73553	0.5981	1.08433	3.67974	3.17984
					0.2	1.97455	0.6561	1.01678	3.28644	3.80453
					0.4	1.97543	0.6636	1.01986	3.14334	3.80875
					0.8	1.97543	0.6711	1.02556	3.06427	3.80435

resistance to rotational motion, making the fluid less susceptible to angular motion. Fig. 7(a and b) exposes the microorganism profile $\chi(\eta)$ under the influence of Peclet number Pe and bioconvective Lewis number Lb. Both parameter effectively reduces the microorganism profile $\chi(\eta)$. The resistance in $\chi(\eta)$ due to Pe is associated to low motile diffusivity.

Table 2 aims to presents the numerical results for skin friction, Nusselt number, Sherwood number and motile density subject to higher values of flow parameters. The wall shear force is influenced with Hartmann numbr and porosity constant. These observations are important for controlling the surface friction. The micro-rotational velocity, representing the angular velocity of micropolar fluid remain stable with minor fluctuations when micropolar fluid parameter α vary. Such stable outcomes in micro-rotational velocity reveals that the rotational dynamic of nanofluid is influenced with Hartmann number while the change near the surface is negligible. The Nusselt number, Sherwood number and motile density number reduces due to Hartmann number M while Prandtl number Pr and stretching constant λ showing increasing impact on these physical quantities.

6. Conclusions

This analysis provides comprehensive analysis for applications of bioconvection in Casson-Micropolar nanofluid flow endorsed by bidirectional moving surface. Modified expressions of Cattaneo-Christov model are used to model the energy and concentration equations. Additional impact of thermal radiation and chemical reaction were attributed. Major observations are.

- ➢ The Casson fluid parameter and porosity parameter reduces the fluid velocity.
- ➢ The micro-rotational velocity enhances when the effects of stretching parameter are prominent. However, porosity parameter controls the micro-rotational velocity.
- ➢ Higher thermal relaxation parameter leads to reduction of temperature profile.
- ➢ The Brownian parameter increases the temperature profile.
- ➢ Presence of porosity parameter and Biot number increases the heat transfer impact.
- ➢ Change in micropolar fluid parameter enhances the thermal profile.
- ➢ The micro-rotation distribution reduces due to micropolar parameter.
- ➢ The concentration profile grows due to thermophoretic parameter while reverse effects are observed for concentration relaxation parameter and chemical reaction constant.

CRediT authorship contribution statement

Rejab Hajlaoui: Writing – review & editing, Writing – original draft, Methodology, Investigation, Formal analysis, Conceptualization. **Aaqib Majeed:** Writing – review & editing, Writing – original draft, Methodology, Investigation, Funding acquisition, Conceptualization. **Sami Ullah Khan:** Writing – review & editing, Writing – original draft, Methodology, Investigation, Formal analysis, Conceptualization.

Mohamed Mahdi Boudabous: Writing – review & editing, Writing – original draft, Methodology, Investigation, Formal analysis, Conceptualization. **Alaa Chabir:** Writing – review & editing, Writing – original draft, Methodology, Investigation, Formal analysis, Conceptualization. **Ali Chamkha:** Writing – review & editing, Writing – original draft, Methodology, Investigation, Conceptualization. **Lioua Kolsi:** Writing – review & editing, Writing – original draft, Methodology, Investigation, Formal analysis, Conceptualization.

Limitation of model

Current model is based on theoretical flow assumptions instead experimental data. Therefore, these exists some minor fluctuation between theoretical and experimental results.

Applications of problem

The claimed observations present applications in optimizing thermal efficiency of various engineering systems, nuclear energy, chemical reactions, cooling technologies, energy storage systems, biomedical devices, fertilizers etc.

Future recommendations

The current results can be modified further by performing the entropy generation effects, Hall features, nonlinear radiated effects and viscous dissipation features. The analysis could be further modified by utilizing the hybrid nanofluid and tri hybrid nanofluid models.

Data availability statement

No external data associated in the work.

Acknowledgment

This research has been funded by Scientific Research Deanship at University of Ha'il, Saudi Arabia through project number RG-24 029.

References

Abbas, N., Shatanawi, W., Rehman, K. U., & Shatnawi, T. A. M. (2024). Velocity and thermal slips impact on boundary layer flow of micropolar nanofluid over a vertical nonlinear stretched Riga sheet. *Proceedings - Institution of Mechanical Engineers, Part N: Journal of Nanomaterials, Nanoengineering and Nanosystems, 238*(3–4), 107–117.

Abdal, S., Hussain, S., Siddique, I., Ahmadian, A., & Ferrara, M. (2021). On solution existence of MHD Casson nanofluid transportation across an extending cylinder through porous media and evaluation of priori bounds. *Scientific Reports, 11*(1), 1–16.

Ali, L., Liu, X., Ali, B., Mujeed, S., Abdal, S., & Mutahir, A. (2020). The impact of nanoparticles due to applied magnetics dipole in micropolar fluid flow using the finite element method. *Symmetry, 12*(4), 520.

Ali, B., Naqvi, R. A., Ali, L., Abdal, S., & Hussain, S. (2021). A comparative description on time-dependent rotating magnetic transport of a water base liquid H2O with hybrid nano-materials Al2O3-Cu and Al2O3-TiO2 over an extending sheet using Buongiorno model: Finite element approach. *Chinese Journal of Physics, 70*, 125–139.

Ameer Ahammad, N., Ahmed, A., Alhowaity, A., Sarfraz, M., Hamam, H., & Galal, A. M. (2022). Convective transport via thermophoresis and brownian forces in MHD Hiemenz stagnation-point flow. *International Journal of Modern Physics B, 36*(29), Article 2250203.

Ariel, P. D. (2007). The three-dimensional flow past a stretching sheet and the homotopy perturbation method. *Computers & Mathematics with Applications, 54*, 920–925.

Baazeem, A. S., Nawaz, Y., & Arif, M. S. (2023). Finite difference modeling of time fractal impact on unsteady magneto-hydrodynamic Darcy–forchheimer flow in non-Newtonian nanofluids with the q-derivative. *Fractal and Fractional, 8*(1), 8.

Batool, M., Akhter, S., Ahmad, S., Ashraf, M., & Ali, K. (2023). Impact of viscous dissipation on MHD Darcy-forchheimer nanoliquid flow comprising gyrotactic microorganisms past a nonlinear extending surface. *30*(6), 2235–2244.

Chabani, I., Mebarek-Oudina, F., Vaidya, H., & Ismail, A. I. (2022). Numerical analysis of magnetic hybrid Nano-fluid natural convective flow in an adjusted porous trapezoidal enclosure. *Journal of Magnetism and Magnetic Materials, 564*, Article 170142.

Choi, S. U., & Eastman, J. A. (1995). *Enhancing thermal conductivity of fluids with nanoparticles (No. ANL/MSD/CP-84938; CONF-951135-29)*. Argonne, IL (United States): Argonne National Lab.(ANL).

Chukami, B. S., & Heyhat, M. M. (2023). Numerical investigation on the effect of Al2O3-water nanofluid on direct steam generation in parabolic trough collectors. *Applied Thermal Engineering*, Article 122300.

Das, S., Karmakar, P., Das, S., & Dinarvand, S. (2025). AI-led study of dynamic changes in milk containing hybrid nanoparticles in an electromagnetically vibrated channel subjected to thermal oscillations and rapid pressure changes: Implications for dairy industry. *Chinese Journal of Physics, 93*, 271–309.

Das, S., Karmakar, P., Pal, T. K., Sarkar, S., Ali, A., & Jana, R. N. (2024). Chemical dynamics in a radioactive platinum-cerium oxide-water mixture within a vibrating Riga channel subject to sudden pressure gradient onset. *Journal of Mathematical Chemistry, 62*(7), 1727–1778.

Eswaramoorthi, S., Nasir, S., Loganathan, K., Satyanarayana Gupta, M., & Berrouk, A. (2025). Numerical simulation of rotating flow of CNT nanofluids with thermal radiation, ohmic heating, and autocatalytic chemical reactions. *Alexandria Engineering Journal, 113*, 535–550.

Guedri, K., Mahmood, Z., Fadhl, B. M., Makhdoum, B. M., Eldin, S. M., & Khan, U. (2023). Mathematical analysis of nonlinear thermal radiation and nanoparticle aggregation on unsteady MHD flow of micropolar nanofluid over shrinking sheet. *Heliyon, 9*(3), Article e14248.

Habib, D., Abdal, S., Ali, R., Baleanu, D., & Siddique, I. (2021). On bioconvection and mass transpiration of micropolar nanofluid dynamics due to an extending surface in existence of thermal radiations. *Case Studies in Thermal Engineering, 27*, Article 101239.

Hayat, T., Farwa, H., Ahmed, A., & Bashir, A. (2020). Unsteady flow of nanofluid through porous medium with variable characteristics. *International Communications in Heat and Mass Transfer, 119*, Article 104904.

Karmakar, P., & Das, S. (2025). AI-powered computational analysis of dynamic responses in a vibrating Riga sensor within a reactive platinum-cerium oxide-water mixture. *Sensors and Actuators A: Physical, 381*, Article 116028.

Karmakar, P., Das, S., Jana, R. N., & Makinde, O. D. (2024). Dynamic response of a weakly ionized fluid in a vibrating Riga channel exposed to intense electromagnetic rotation. *Microfluidics and Nanofluidics, 28*(10), 70.

Karvelas, E. G., Tsiantis, A., & Papathanasiou, T. D. (2020). Effect of micropolar fluid properties on the hydraulic permeability of fibrous biomaterials. *Computer Methods and Programs in Biomedicine, 185*, Article 105135.

Khan, S. A., Ali, B., Eze, C., Lau, K. T., Ali, L., Chen, J., & Zhao, J. (2021). Magnetic dipole and thermal radiation impacts on stagnation point flow of micropolar based nanofluids over a vertically stretching sheet: Finite element approach. *Processes, 9*(7), 1089.

Loganathan, K., Choudhary, P., Eswaramoorthi, S., Senthilvadivu, K., Thamaraikannan, N., & Reema, J. (2025). Implications of entropy generation in bioconvective flow on Maxwell nanofluid past a Riga plate with Cattaneo–Christov model. *Partial Differential Equations in Applied Mathematics, 13*, Article 101077.

Loganathan, K., Thamaraikannan, N., Eswaramoorthi, S., & Reema, J. (2025). Entropy framework of the bioconvective Williamson nanofluid flow over a Riga plate with radiation, triple stratification and swimming microorganisms. *International Journal of Thermofluids, 25*, Article 101000.

Mahanthesh, B., Gireesha, B. J., & Gorla, R. S. (2016). Mixed convection squeezing three-dimensional flow in a rotating channel filled with nanofluid. *International Journal of Numerical Methods for Heat and Fluid Flow, 26*(5), 1460–1485.

Mahian, O., Bellos, E., Markides, C. N., Taylor, R. A., Alagumalai, A., Yang, L., & Wongwises, S. (2021). Recent advances in using nanofluids in renewable energy systems and the environmental implications of their uptake. *Nano Energy, 86*, Article 106069.

Mahmood, Z., Alhazmi, S. E., Alhowaity, A., Marzouki, R., Al-Ansari, N., & Khan, U. (2022). MHD mixed convective stagnation point flow of nanofluid past a permeable stretching sheet with nanoparticles aggregation and thermal stratification. *Scientific Reports, 12*(1), Article 16020.

Majeed, A., Khan, S. U., Abbas, T., Ijaz Khan, M., Sayfutdinovna Abdullaeva, B., Ismail, E. A., & Awwad, F. A. (2024). Bidirectional bioconvective flow of Casson–micropolar nanofluid due to porous Riga surface with heat generation effects. *AIP Advances, 14*, Article 115214.

Mashhadian, A., Heyhat, M. M., & Mahian, O. (2021). Improving environmental performance of a direct absorption parabolic trough collector by using hybrid nanofluids. *Energy Conversion and Management, 244*, Article 114450.

Muhammad, K., Sarfraz, M., Ameer Ahammad, N., & Elseesy, I. E. (2025). Improving thermal efficiency through Cu-MoS2 hybrid nanomaterials: A numerical and statistical approach. *Chaos, Solitons & Fractals, 192*, Article 116014.

Nasir, S., Berrouk, A. S., Gul, T., Zari, I., Alghamdi, W., & Ali, I. (2023). Unsteady mix convectional stagnation point flow of nanofluid over a movable electro-magnetohydrodynamics Riga plate numerical approach. *Scientific Reports, 13*(1), Article 10947.

Pandey, S. K., & Chandra, S. (2020). Transportation of micro-polar fluid by dilating peristaltic waves. *Journal of King Saud University Science, 32*(7), 2939–2949.

Rajput, S., Bhattacharyya, K., Pandey, A. K., & Chamkha, A. J. (2022). Unsteady axisymmetric flow of nanofluid on nonlinearly expanding surface with variable fluid properties. *JCIS open, 8*, Article 100064.

Ramasekhar, G., & Bala Anki Reddy, P. (2023). Entropy generation on Darcy–Forchheimer flow of Copper-Aluminium oxide/Water hybrid nanofluid over a rotating disk: Semi-analytical and numerical approaches. *Scientia Iranica, 30*(6), 2245–2259, 2023.

Rana, S., Nawaz, M., Saleem, S., & Alharbi, S. O. (2020). Numerical study on enhancement of heat transfer in hybrid nano-micropolar fluid. *Physica Scripta, 95*(4), Article 045201.

Sarfraz, M., & Khan, M. (2023a). Magnetized homann flow comprising GO and Co3O4 nanoparticles past a biaxially stretching surface. *Physica Scripta, 98*(3), Article 035218.

Sarfraz, M., Yasir, M., & Khan, M. (2023). Exploring dual solutions and thermal conductivity in hybrid nanofluids: A comparative study of Xue and Hamilton–crosser models. *Nanoscale Advances, 5*(23), 6695–6704.

Senthilvadivu, K., Eswaramoorthi, S., Loganathan, K., & Nazek, A. (2024). Impact of thermal energy on water and ethylene glycol (50: 50)-Based rotating hybrid nanofluid past A Riga surface with radiation, homogeneous and heterogeneous reactions. *Nano*, Article 2450162.

Thriveni, K., & Mahanthesh, B. (2021). Significance of variable fluid properties on hybrid nanoliquid flow in a micro-annulus with quadratic convection and quadratic thermal radiation: Response surface methodology. *International Communications in Heat and Mass Transfer, 124*, Article 105264.

Yasir, M., Khan, M., Ahmed, A., & Sarfraz, M. (2023). Flow of Oldroyd-B nanofluid in non-inertial frame inspired by Cattaneo-Christov theory. *Waves in Random and Complex Media*, 1–12.

Zaheer, M., Abbas, S. Z., Huang, N., & Elmasry, Y. (2024). Analysis of buoyancy features on magneto hydrodynamic stagnation point flow of nanofluid using homotopy analysis method. *International Journal of Heat and Mass Transfer, 221*, Article 125045.

Glossary

(u, v, w): velocity components (ms^{-1})
(x, y, z): coordinates (m)
ρ_f: density (kgm^{-3})
λ_0: thermal relaxation coefficient (s)
D_T: thermophoretic coefficient (m^2s^{-1})
T: temperature (K)
T_∞: free stream temperature (K)
C: dilute concentration (kgm^{-3})
C_∞: ambient stream concentration (kgm^{-3})
Nb: Brownian motion (m^2s^{-1})
σ: electric conductivity
K: micropolar fluid coefficient
ω: Casson fluid coefficient
q_r: radiated coefficient
K^*: porous media coefficient
K_*: reaction coefficient
j: microintertia density
D_m: microorganisms diffusivity
$\overline{b}$: chemotaxis constant
w_c: maximum cells speed
N: micro-rotation
n: microorganisms density
(N_1, N_2): micro-angular speed
n_∞: ambient microorganism density
α: micropolar parameter
M: Hartmann number
λ: stretching parameter
Pr: Prandtl number
Nt: thermophoresis parameter
Sc: Schmidt number
Pe: Peclet number (Pe)